A Pointwise Minimum Norm Control Scheme for a Generic Air-Breathing Hypersonic Vehicle

Research Project 2, Course #085852

Omer Wexler

Advisor: Moshe Idan
Department of Aerospace Engineering, Haifa, Israel.

April, 2025

This project focuses on the application of a nonlinear, pointwise minimum norm control law for air-breathing hypersonic vehicles. Its goal is to stabilize the aircraft about trim conditions with and without a canard. The theory behind the control scheme is presented and discussed, alongside relevant conditions. Several models for the aircraft are introduced: a high-fidelity model and two control-oriented models, which are used for design. Controller forms of both models are derived, and a control strategy is constructed and evaluated in numerical simulations.

Nomenclature

α	Angle of attack
α_V	Desired negativity function
β_i	ith thrust fit parameter
$\mathbf{0}$	Zero matrix
$\boldsymbol{I}$	Identity matrix
δ_c	Abstract canard deflection
δ_e	Abstract elevator deflection
γ	Flight path angle
$\mathcal{L}$	Lie derivative
$\overline{c}$	Mean aerodynamic chord
Φ	Stoichiometrically normalized fuel-to-air ratio
$\Phi(\vec{x})$	Diffeomorphism transformation function
Φ_c	Dynamic extension command signal
ψ_0	Pointwise minimum norm switching function
ρ	Air density
θ	Pitch angle
$\tilde{u}$	Input pertubations from trim conditions
$\tilde{x}$	State pertubations from trim conditions
ε	Desired negativity parameter
$\vec{\psi}_1$	Pointwise minimum norm direction function
$\vec{\xi}$	Controller form diffeomorphism states

$\vec{l}_0$ Non-linear, free terms in controller form derivatives

$\vec{u}_t$ Control inputs at trim conditions

$\vec{u}$ Control inputs

$\vec{x}_t$ State space states at trim conditions

$\vec{x}$ State space states

$\vec{y}$ State space outputs

c_c Canard coefficient of moment

C_D Coefficient of drag

C_D^0 Constant drag coefficient

$C_D^{\alpha^i}$ ith order coefficient of α contribution to C_D

$C_D^{\delta_c^i}$ ith order coefficient of δ_c contribution to C_D

$C_D^{\delta_e^i}$ ith order coefficient of δ_e contribution to C_D

c_e Elevator coefficient of moment

C_L Coefficient of lift

C_L^0 Constant lift coefficient

C_L^{α} Coefficient of α contribution to C_L

$C_L^{\delta_c^i}$ ith order coefficient of δ_c contribution to C_L

$C_L^{\delta_e^i}$ ith order coefficient of δ_e contribution to C_L

C_M Coefficient of moment

C_M^0 Constant pitching moment coefficient

$C_M^{\alpha^i}$ ith order coefficient of α contribution to C_M

C_T^0 Constant thrust coefficient

$C_T^{\alpha^i}$ ith order coefficient of α contribution to thrust

D Drag

F Coefficient matrix of linear state derivatives in controller form

G Coefficient matrix of nonlinear state derivatives in controller form

g Gravitation constant

h Height

I_y Longitudinal moment of inertia

L Lift

l_1 Control inputs coefficient matrix in controller form derivatives

M Pitching moment

m Vehicle mass

P Algebraic Riccati equation solution

Q Algebraic Riccati equation coefficient matrix, or Pitch rate (depends on context)

q Dynamic pressure

R Algebraic Riccati equation coefficient matrix

S Reference area

T Thrust

V Air speed (magnitude)

$V(\vec{\xi})$ Robust control Lyaponuv function

z_T Thrust to moment coupling coefficient

I. Introduction

In recent years, the application of air-breathing hypersonic vehicles (AHVs) in civil and military fields has become the center of attention of many institutes and countries alike. Such vehicles are highly unstable and nonlinear in nature, introducing a complex set of challenges that must be overcome to control them. These intricate characteristics, alongside their promising capabilities, instigate interest in AHVs.

This project is part of ongoing research regarding control systems of AHVs. Its goal is to assess the performance of the pointwise minimum norm (PMN) control law [1] (chapter 4.2.3) when applied to a generic longitudinal AHV model [2]. Within the scope of this work, the objective is to stabilize the vehicle about its trim conditions. Tracking problems were not considered at this stage and will be addressed in subsequent research efforts. The following work builds on knowledge and infrastructure developed in [3]. Previous developments include key findings such as model reconstruction and validation, trim conditions, symbolic and numeric utility functions, as well as knowledge regarding the control challenges of this field. Thus, these topics will not be discussed at the same level of detail.

First, the PMN law is presented for feedback linearizable systems. The controller design process and conditions for its validity are discussed, as well as the relevant formulas. A specific case of the PMN law is considered: a feedback linearizable system with no disturbances. More information on alternative forms and the addition of disturbances can be found in [1]. The controller's effectiveness is mathematically demonstrated over an arbitrary robust control Lyapunov function (RCLF) [1].

Then, mathematical models of a generic AHV are introduced [2]. The first is a curve-fitted model (CFM) based on a high-fidelity truth model (TM). From the CFM, two additional models are derived: the extended control-oriented model (ECOM) and the canard control-oriented model (CCOM). The former utilizes a second-order dynamic extension and disregards the canard to reduce the number of control inputs in effect. The latter incorporates the canard but doesn't require a dynamic extension for transition to controller form. Both neglect some characteristics of the CFM, which will be considered as perturbations.

Finally, the transformation to the controller form of both systems is derived, and the PMN law is applied to them. Final results are shown, and the controller performance is evaluated at and around trim conditions. Then, based on those findings, future work and research will be addressed.

II. The Pointwise Minimum Norm Control Law

Assume that a diffeomorphism $\vec{\xi} = \Phi(\vec{x})$, $\Phi(\vec{0}) = \vec{0}$ exists such that an arbitrary system $\dot{\vec{x}} = f(\vec{x}, \vec{u}, t)$ can be transformed into

$$\dot{\vec{\xi}} = F\vec{\xi} + G\left[\vec{l}_0\left(\vec{\xi}\right) + l_1\left(\vec{\xi}\right)\vec{u}\right]. \tag{1}$$

The matrix pair (F, G) is assumed to be controllable, the continuous functions $\vec{l}_0, l_1$ satisfy $\vec{l}_0(\vec{0}) = \vec{0}$ and $l_1(\vec{\xi})$ must be nonsigular. Let P be the symmetric PD solution of the Riccati equation,

$$F^T P + PF - PGR^{-1}G^T P + Q = 0, \quad Q, R > 0. \tag{2}$$

In such a case, the function $V(\vec{x}) = \Phi(\vec{x})^T P\Phi(\vec{x}) = \vec{\xi}^T P\vec{\xi}$ is a respective RCLF with $\alpha_V(\vec{x}) = \varepsilon\vec{\xi}^T Q\vec{\xi}$ for some $\varepsilon \in (0, 1)$ [1]. α_V acts as a design parameter. It outlines the desired upper bound of the

RCLF derivative along the solution. The Lie derivatives of V are

$$\mathcal{L}_f V(\vec{\xi}) = \vec{\xi}^T \left[F^T P + PF\right] \vec{\xi} + 2\vec{\xi}^T PG\vec{l}_0(\vec{\xi}), \quad \mathcal{L}_g V(\vec{\xi}) = 2\vec{\xi}^T PGl_1(\vec{\xi}). \tag{3}$$

Define

$$\psi_0(\vec{\xi}) = \mathcal{L}_f V(\vec{\xi}) + \alpha_V(\vec{\xi}) = \mathcal{L}_f V(\vec{\xi}) + \varepsilon\vec{\xi}^T Q\vec{\xi}, \quad \vec{\psi}_1(\vec{\xi}) = \left[\mathcal{L}_g V(\vec{\xi})\right]^T. \tag{4}$$

The proposed PNM controller is * [1]

$$u(\vec{\xi}) = \begin{cases} -\dfrac{\psi_0(\vec{\xi})\vec{\psi}_1(\vec{\xi})}{\vec{\psi}_1^T(\vec{\xi})\vec{\psi}_1(\vec{\xi})} & , \psi_0(\vec{\xi}) > 0 \\ 0 & , \psi_0(\vec{\xi}) \leq 0 \end{cases} = \begin{cases} -\dfrac{\psi_0(\vec{\xi})l_1^T(\vec{\xi})G^T P\vec{\xi}}{2\vec{\xi}^T PGl_1(\vec{\xi})l_1^T(\vec{\xi})G^T P\vec{\xi}} & , \psi_0(\vec{\xi}) > 0 \\ 0 & , \psi_0(\vec{\xi}) \leq 0 \end{cases}. \tag{5}$$

This is a specific implementation of the PMN law. It could be applied to a more generalized set of systems and account for disturbances. Moreover, it is optimal with respect to a meaningful cost function.

To demonstrate the effectiveness of this controller, examine the following RCLF candidate (under the assumptions listed above),

$$V(\vec{\xi}) = \vec{\xi}^T P\vec{\xi}. \tag{6}$$

Its time derivative is

$$\dot{V}(\vec{\xi}) = \mathcal{L}_f V(\vec{\xi}) + \mathcal{L}_g V(\vec{\xi})\vec{u} = -\varepsilon\vec{\xi}^T Q\vec{\xi} + \psi_0 + \vec{\psi}_1^T\vec{u}. \tag{7}$$

Considering the PMN law (5), when ψ_0 is non-positive, it is guaranteed that $\dot{V} \leq -\varepsilon\vec{\xi}^T Q\vec{\xi} < 0$. This is ensured by Q being positive definite. If ψ_0 is positive, then $\vec{u}$ is determined by the top expression in (5), meaning, the time derivative of V is

$$\dot{V}(\vec{\xi}) = -\varepsilon\vec{\xi}^T Q\vec{\xi} + \psi_0 + \vec{\psi}_1^T \left(-\frac{\psi_0\vec{\psi}_1}{\vec{\psi}_1^T\vec{\psi}_1}\right) = -\varepsilon\vec{\xi}^T Q\vec{\xi} + \psi_0 - \psi_0\frac{\vec{\psi}_1^T\vec{\psi}_1}{\vec{\psi}_1^T\vec{\psi}_1} = -\varepsilon\vec{\xi}^T Q\vec{\xi}. \tag{8}$$

To conclude, applying the PMN law entails that

$$\dot{V}(\vec{\xi}) \leq -\varepsilon\vec{\xi}^T Q\vec{\xi}. \tag{9}$$

In effect, this mechanism activates a control signal only if it is required at the moment (pointwise). If the system is in a state where the RCLF inherently converges to zero, the control is off (minimum norm). Otherwise, a controller is applied such that $\dot{V}(\vec{\xi})$ is held at the upper bound $-\alpha_V = -\varepsilon\vec{\xi}Q\vec{\xi} < 0$.

*** *A Warning Sign* - When implementing (5), take extreme caution. A small mistake could be disastrous, as the author of this document could testify. For the sake of one's mental sanity, use the generalized definition on the left of (5).**

III. Curve-Fitted AHV Model

This work considers the CFM model proposed in [2]. It is based on a rich truth model, which is also mentioned in the same article, but not in full detail. Its geometry is depicted in Fig. 1. The

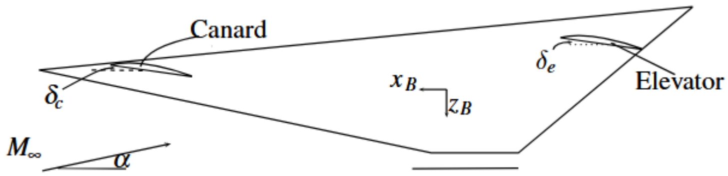

Fig. 1 Geometry of the AHV.

CFM encapsulates aerodynamic forces and thrust via

$$
\begin{aligned}
L \approx \frac{1}{2}\rho V^2 S C_L(\alpha, \delta_e, \delta_c), \quad M \approx z_T T + \frac{1}{2}\rho V^2 S\bar{c} C_M(\alpha, \delta_e, \delta_c),\\
D \approx \frac{1}{2}\rho V^2 S C_D(\alpha, \delta_e, \delta_c), \quad T \approx \alpha^3 C_T^{\alpha^3}(\Phi) + \alpha^2 C_T^{\alpha^2}(\Phi) + \alpha C_T^{\alpha}(\Phi) + C_T^{0}(\Phi).
\end{aligned}
\tag{10}
$$

The normalized coefficients are of the following form,

$$
\begin{gathered}
C_L = C_L^{\alpha}\alpha + C_L^{\delta_e}\delta_e + C_L^{\delta_c}\delta_c + C_L^0, \quad C_D = C_D^{\alpha^2}\alpha^2 + C_D^{\alpha}\alpha + C_D^{\delta_e^2}\delta_e^2 + C_D^{\delta_e}\delta_e + C_D^{\delta_c^2}\delta_c^2 + C_D^{\delta_c}\delta_c + C_D^0,\\
C_M = C_M^{\alpha^2}\alpha^2 + C_M^{\alpha}\alpha + C_M^0 + c_e\delta_e + c_c\delta_c,\\
C_T^{\alpha^3} = \beta_1(h,q)\Phi + \beta_2(h,q), \quad C_T^{\alpha^2} = \beta_3(h,q)\Phi + \beta_4(h,q),\\
C_T^{\alpha} = \beta_5(h,q)\Phi + \beta_6(h,q), \quad C_T^{0} = \beta_7(h,q)\Phi + \beta_8(h,q).
\end{gathered}
\tag{11}
$$

All relevant constants are listed in Appendix A. Note that while β_i changes with altitude and dynamic pressure, these functions are assumed to be constant during standard operation, or at least change at slow rates. The equations of motion for this model are

$$
\begin{gathered}
\vec{x} = \begin{Bmatrix} V & \alpha & Q & \theta \end{Bmatrix}^T, \quad \vec{u} = \begin{Bmatrix} \delta_e & \Phi & \delta_c \end{Bmatrix}^T, \quad \vec{y} = \begin{Bmatrix} V & \gamma \end{Bmatrix}^T = \begin{Bmatrix} V & \theta - \alpha \end{Bmatrix}^T,\\
\begin{Bmatrix} \dot{V} \\ \dot{\alpha} \\ \dot{Q} \\ \dot{\theta} \end{Bmatrix} = \begin{Bmatrix} \dfrac{1}{m}\Big(T\cos(\alpha) - D\Big) - g\sin(\theta - \alpha) \\ \dfrac{1}{mV}\Big(-T\sin(\alpha) - L\Big) + Q + \dfrac{g}{V}\cos(\theta - \alpha) \\ \dfrac{M}{I_y} \\ Q \end{Bmatrix}.
\end{gathered}
\tag{12}
$$

The original formulation includes additional flexible states, which will not be mentioned here.

IV. Control-Oriented Models

A. Extended Control-Oriented Model

While the CFM proposes three controllers (δ_e, δ_c, and Φ), it is preferable to use as few as possible. Therefore, in this model, the canard is removed. It is also simulated accordingly. The ECOM [†] is obtained when neglecting elevator couplings ($C_L^{\delta_e}$, $C_D^{\delta_e^2}$, $C_D^{\delta_e}$), and the flexible states (that will not be mentioned in detail in this paper). Flight altitude is assumed to be constant, and a dynamic extension over Φ is added. The relevant equations of motion describing the ECOM are [2]

$$\vec{x} = \begin{Bmatrix} V & \alpha & Q & \theta \end{Bmatrix}^T, \quad \vec{u} = \begin{Bmatrix} \delta_e & \Phi \end{Bmatrix}^T, \quad \vec{y} = \begin{Bmatrix} V & \gamma \end{Bmatrix}^T = \begin{Bmatrix} V & \theta - \alpha \end{Bmatrix}^T,$$
$$\begin{Bmatrix} \dot{V} \\ \dot{\alpha} \\ \dot{Q} \\ \dot{\theta} \end{Bmatrix} = \begin{Bmatrix} \frac{1}{m}\Big(T\cos(\alpha) - D\Big) - g\sin(\theta-\alpha) \\ \frac{1}{mV}\Big(-T\sin(\alpha) - L\Big) + Q + \frac{g}{V}\cos(\theta-\alpha) \\ \frac{M}{I_y} \\ Q \end{Bmatrix}. \tag{13}$$

Note that the outputs of this model are selected to be V and γ. Recall that elevator couplings with D and L were neglected, restricting the authority of δ_e exclusively to C_{M,δ_e}. It is included in the model through M (directly), which affects the derivative $\dot{Q}$. Since the measurement $\gamma = \theta - \alpha$, it can be shown that the control input δ_e appears only in the third time-derivative of γ, meaning it has a relative degree of 3. Φ, on the other hand, will appear in the first derivative of V through T, making its relative degree 1.

This mismatch between δ_e and Φ in relative degree will invalidate the transition to controller form. Therefore, a dynamic extension over Φ is added. It introduces the control input Φ_c, and states Φ and $\dot{\Phi}$. These new states are associated with a second-order actuator

$$\ddot{\Phi} = -2\zeta\omega\dot{\Phi} - \omega^2\Phi + \omega^2\Phi_c. \tag{14}$$

Denote the model states and inputs as

$$\vec{x} = \begin{Bmatrix} x_1 & x_2 & x_3 & x_4 & x_5 & x_6 \end{Bmatrix}^T = \begin{Bmatrix} V & \alpha & Q & \theta & \Phi & \dot{\Phi} \end{Bmatrix}^T, \quad \vec{u} = \begin{Bmatrix} u_1 & u_2 \end{Bmatrix}^T = \begin{Bmatrix} \delta_e & \Phi_c \end{Bmatrix}^T. \tag{15}$$

[†]This model is denoted COM in [2], here it is called "extended" due to the dynamic extension.

Applying this notation, and appending the state-space form of (14) to (13) yields

$$\vec{x} = \begin{Bmatrix} x_1 & x_2 & x_3 & x_4 & x_5 & x_6 \end{Bmatrix}^T, \quad \vec{u} = \begin{Bmatrix} u_1 & u_2 \end{Bmatrix}^T, \quad \vec{y} = \begin{Bmatrix} x_1 & x_4 - x_2 \end{Bmatrix}^T,$$

$$\dot{\vec{x}} = \begin{Bmatrix} f_1(\vec{x},\vec{u}) \\ f_2(\vec{x},\vec{u}) \\ f_3(\vec{x},\vec{u}) \\ f_4(\vec{x},\vec{u}) \\ f_5(\vec{x},\vec{u}) \\ f_6(\vec{x},\vec{u}) \end{Bmatrix} = \begin{Bmatrix} \frac{1}{m}\Big(T(\vec{x},\vec{u})\cos(x_2) - D(\vec{x},\vec{u})\Big) - g\sin(x_4 - x_2) \\ \frac{1}{mx_1}\Big(-T(\vec{x},\vec{u})\sin(x_2) - L(\vec{x},\vec{u})\Big) + x_3 + \frac{g}{x_1}\cos(x_4 - x_2) \\ \frac{M(\vec{x},\vec{u})}{I_{yy}} \\ x_3 \\ x_6 \\ -2\zeta\omega x_6 - \omega^2 x_5 + \omega^2 \Phi_c \end{Bmatrix}. \tag{16}$$

This form has six states and two control inputs, which possess a relative degree of three, meaning it has a full vector relative degree. The trim conditions of this model were addressed in [3] and are summarized in Table 1.

Table 1 Trim conditions of the ECOM at level flight, a speed of 7702.0808 [ft/s], and a height of 85000 [ft].

State/Input	Value	Units
V	7702.0808	ft/s
α	3.684	deg
Q	0	deg/s
V	3.684	deg
Φ	0.1619	—
$\dot{\Phi}$	1/s	
δ_e	16.368	deg
Φ_c	0.1619	—

B. Canard Control-Oriented Model

When utilizing the canard, the problem takes a different shape, which eases the application of some control schemes. The CCOM is obtained by making similar assumptions to the ECOM: neglecting nonlinear control surface couplings ($C_D^{\delta_e^2}$, $C_D^{\delta_c^2}$), and the flexible states. Flight altitude is assumed to be constant. The relevant equations of motion describing the CCOM are [2]

$$\vec{x} = \begin{Bmatrix} x_1 & x_2 & x_3 & x_4 \end{Bmatrix}^T = \begin{Bmatrix} V & \alpha & Q & \theta \end{Bmatrix}^T, \quad \vec{y} = \begin{Bmatrix} x_1 & x_4 - x_2 \end{Bmatrix}^T = \begin{Bmatrix} V & \theta - \alpha \end{Bmatrix}^T,$$
$$\vec{u} = \begin{Bmatrix} u_1 & u_2 & u_3 \end{Bmatrix}^T = \begin{Bmatrix} \delta_e & \Phi & \delta_c \end{Bmatrix}^T,$$
$$\dot{\vec{x}} = \begin{Bmatrix} f_1(\vec{x},\vec{u}) \\ f_2(\vec{x},\vec{u}) \\ f_3(\vec{x},\vec{u}) \\ f_4(\vec{x},\vec{u}) \end{Bmatrix} = \begin{Bmatrix} \frac{1}{m}\Big(T(\vec{x},\vec{u})\cos(x_2) - D(\vec{x},\vec{u})\Big) - g\sin(x_4 - x_2) \\ \frac{1}{mx_1}\Big(-T(\vec{x},\vec{u})\sin(x_2) - L(\vec{x},\vec{u})\Big) + x_3 + \frac{g}{x_1}\cos(x_4 - x_2) \\ \frac{M(\vec{x},\vec{u})}{I_{yy}} \\ x_3 \end{Bmatrix}. \tag{17}$$

All states (except θ) and outputs have a relative degree of 1, with respect to all controllers. In Table 2 are the trim conditions for this model.

Table 2 Trim conditions of the CCOM at level flight, a speed of 7702.0808 [ft/s], and a height of 85000 [ft].

State/Input	Value	Units
V	7702.0808	ft/s
α	2.224	deg
Q	0	deg/s
V	2.224	deg
δ_e	5.215	deg
Φ	0.1039	—
δ_c	5.770	deg

V. PMN Application to Generic AHV Models

A. Solution Approach

This project aims to demonstrate the use of a PMN law for a generic AHV. It can be used in a plethora of cases, including ones with disturbances. It is assumed that trim conditions are known, and changes in altitude and non-linear aerodynamic coefficients can be regarded as disturbances. Consequently, all the simulations in this work were conducted using the control-oriented models. In addition, the objective will be to stabilize the aircraft in a local environment around trim. Tracking-error dynamics will not be discussed in this work.

B. Extended Control-Oriented Model

In this case, the transition to controller form is not trivial. First, to ensure a single equilibrium point at the origin, define the translated system $\tilde{x}$ and $\tilde{u}$ as

$$\tilde{x} = \vec{x} - \vec{x}_t, \quad \tilde{u} = \vec{u} - \vec{u}_t. \tag{18}$$

The notation $_t$ refers to trim conditions. Denote the state space vector of controller form as $\vec{\xi} \in \mathbb{R}^6$, where $\xi_1 = \tilde{V}$ and $\xi_2 = \tilde{\gamma}$. The remaining four states of $\vec{\xi}$ appear in the Lie derivatives of V and γ, namely

$$\vec{\xi} = \left\{ \tilde{V} \quad \tilde{\gamma} \quad \mathcal{L}_f\tilde{V} \quad \mathcal{L}_f\tilde{\gamma} \quad \mathcal{L}_f^2\tilde{V} \quad \mathcal{L}_f^2\tilde{\gamma} \right\}^T. \tag{19}$$

Recall that this model has a relative degree of three with respect to both inputs and outputs. Therefore, the transition to the controller form is possible. As a direct result of the definition made in (19), the equations of motion for $\vec{\xi}$ are

$$\begin{aligned} \dot{\xi}_1 &= \xi_3, \quad & \dot{\xi}_3 &= \xi_5, \quad & \dot{\xi}_5 &= \mathcal{L}_f^3\tilde{V} + \left(\mathcal{L}_{\Phi_c}\mathcal{L}_f^2\tilde{V}\right)\Phi_c + \left(\mathcal{L}_{\delta_e}\mathcal{L}_f^2\tilde{V}\right)\delta_e, \\ \dot{\xi}_2 &= \xi_4, \quad & \dot{\xi}_4 &= \xi_6, \quad & \dot{\xi}_6 &= \mathcal{L}_f^3\tilde{\gamma} + \left(\mathcal{L}_{\Phi_c}\mathcal{L}_f^2\tilde{\gamma}\right)\Phi_c + \left(\mathcal{L}_{\delta_e}\mathcal{L}_f^2\tilde{\gamma}\right)\delta_e. \end{aligned} \tag{20}$$

The notation $\mathcal{L}_{u_i}\mathcal{L}_f^2 V$ (u_i is either Φ_c or δ_e) refers to the coefficients of the control inputs that are discovered in the higher derivatives. The derivatives $\dot{\xi}_5$ and $\dot{\xi}_6$ in (20) are constructed using a symbolic MATLAB code. In (20), there are four linear derivatives and two non-linear ones involving the control inputs as well. Hence, the controller form of this system is

$$F = \begin{bmatrix} \mathbf{0} & \boldsymbol{I} & \mathbf{0} \\ \mathbf{0} & \mathbf{0} & \boldsymbol{I} \\ \mathbf{0} & \mathbf{0} & \mathbf{0} \end{bmatrix}, \quad G = \begin{bmatrix} \mathbf{0} \\ \mathbf{0} \\ \boldsymbol{I} \end{bmatrix}, \quad \vec{l}_0(\tilde{x}) = \begin{bmatrix} \mathcal{L}_f^3 V \\ \mathcal{L}_f^3\tilde{\gamma} \end{bmatrix}, \quad l_1(\tilde{x}) = \begin{bmatrix} \mathcal{L}_{\delta_e}\mathcal{L}_f^2\tilde{V} & \mathcal{L}_{\Phi_c}\mathcal{L}_f^2\tilde{V} \\ \mathcal{L}_{\delta_e}\mathcal{L}_f^2\tilde{\gamma} & \mathcal{L}_{\Phi_c}\mathcal{L}_f^2\tilde{\gamma} \end{bmatrix}. \tag{21}$$

Due to the definition of $\tilde{x}$, and analysis of this model reported in [3], the origin is an unstable equilibrium of this system, matching $\tilde{u} = 0$. The pair F and G is controllable, making (21) the controller form of the system. Figure 2 depicts the determinant and condition number of $l_1(\tilde{x})$ along admissible flight conditions, demostrating numerically that $l_1(\tilde{x})$ is a non-singular matrix. This was also verified symbolically. The diffeomorphism used to translate $\tilde{x}$ to $\vec{\xi}$ is also validated in the same manner. It is non-singular and globally valid. In addition, simple substitution reveals that $l_0(\vec{0}) = \vec{0}$. Considering these results, the diffeomorphism to controller form and the PMN controller satisfy the required conditions.

Although the theoretical basis is valid, there is some unknown issue with the implementation of this controller, and no concrete results have been obtained. The error stems from a discrepancy between the symbolic expression of $\vec{\psi}_1$ and ψ_0 and their actual values. It could arise from an improper diffeomorphism or derivation of $\vec{\psi}_1$ and ψ_0. Both possibilities are related to implementation.

C. Canard Control-Oriented Model

A significant advantage of the CCOM is its inherent controller form. Due to the linear component in $\dot{x}_4$, it is possible to encapsulate the derivatives of x_1, x_2, and x_3 into a 3×1 vector. Since there are three control inputs that affect three state derivatives, l_1 can be defined as a 3×3 matrix. In

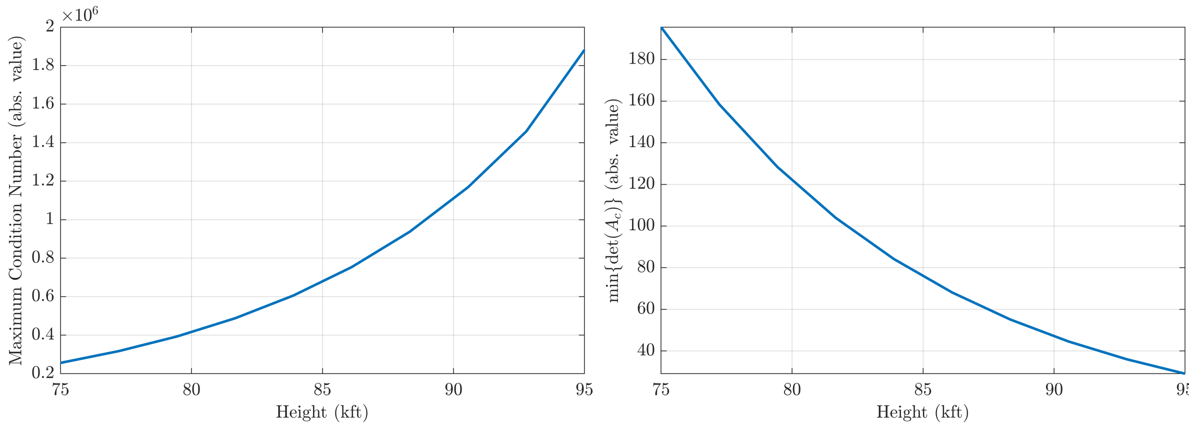

Fig. 2 Condition number and determinant of $l_1(\tilde{x})$ along admissable flight conditions. Matches the ECOM's controller form.

addition, the neglections involved in the CCOM make it affine in control, and the controller form is valid. Respectively, F and G are

$$F = \begin{bmatrix} 0 & 0 & 0 & 0 \\ 0 & 0 & 0 & 0 \\ 0 & 0 & 0 & 0 \\ 0 & 0 & 1 & 0 \end{bmatrix}, \quad G = \begin{bmatrix} 1 & 0 & 0 \\ 0 & 1 & 0 \\ 0 & 0 & 1 \\ 0 & 0 & 0 \end{bmatrix}. \tag{22}$$

All the other terms in $\dot{x}$ are included in $\vec{l}_0$ and l_1. Again, their explicit functions are computed via a symbolic MATLAB code. F and G are a controllable pair, and $\vec{l}_0$ satisfies $\vec{l}_0(\vec{0}) = \vec{0}$. Figure 3 depicts the determinant and condition number of $l_1(\tilde{x})$ along admissible flight conditions. While the condition number is relatively low and the determinant is close to zero, $l_1(\tilde{x})$ is not a singular matrix. It was also verified symbolically. Hence, all the conditions required for the PMN controller are met.

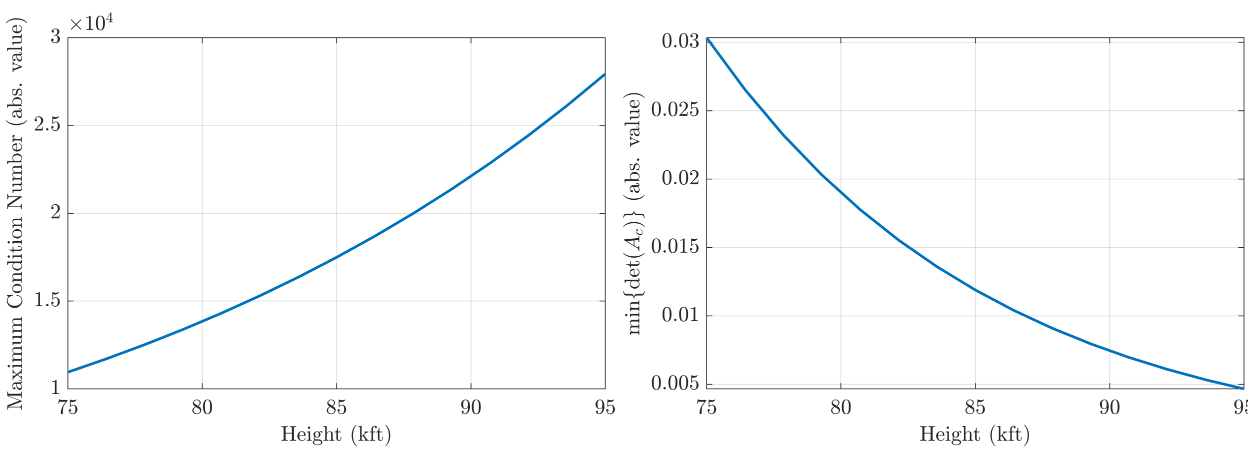

Fig. 3 Condition number and determinant of $l_1(\tilde{x})$ along admissable flight conditions. Matches the CCOM's controller form.

In the current study, the controller design parameters were set to ε is 0.5, and $Q = R = I$. In future work, these parameters can be modified to tune the controller performance.

To validate controller performance, it is first simulated at trim. The resulting system response and control signals are presented in Figs. 4 and 5, respectively. The controller maintains trim conditions, with some numerical errors of minuscule scales. The natural instability of the system causes it to oscillate around trim conditions, and numerical errors arise due to the instability of the system at trim (which constantly pulls it away). Overall, the PMN law can maintain trim. These results match the dynamic characteristics of the underlying RCLF depicted in Fig. 6. It shows that the RCLF, its derivative, and various components oscillate around zero as the system tends to move away from trim, but are contained by the controller.

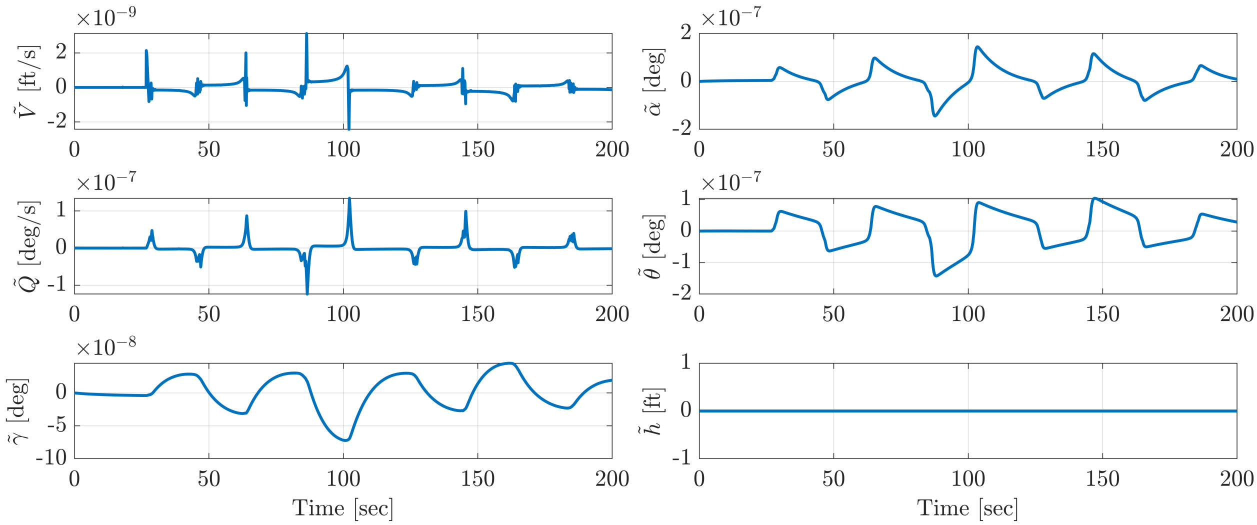

Fig. 4 State errors from trim over time. Simulation is initialized exactly at trim conditions. The model used for simulation is the CCOM. Solved with ode23s (stiff Rosenbrock).

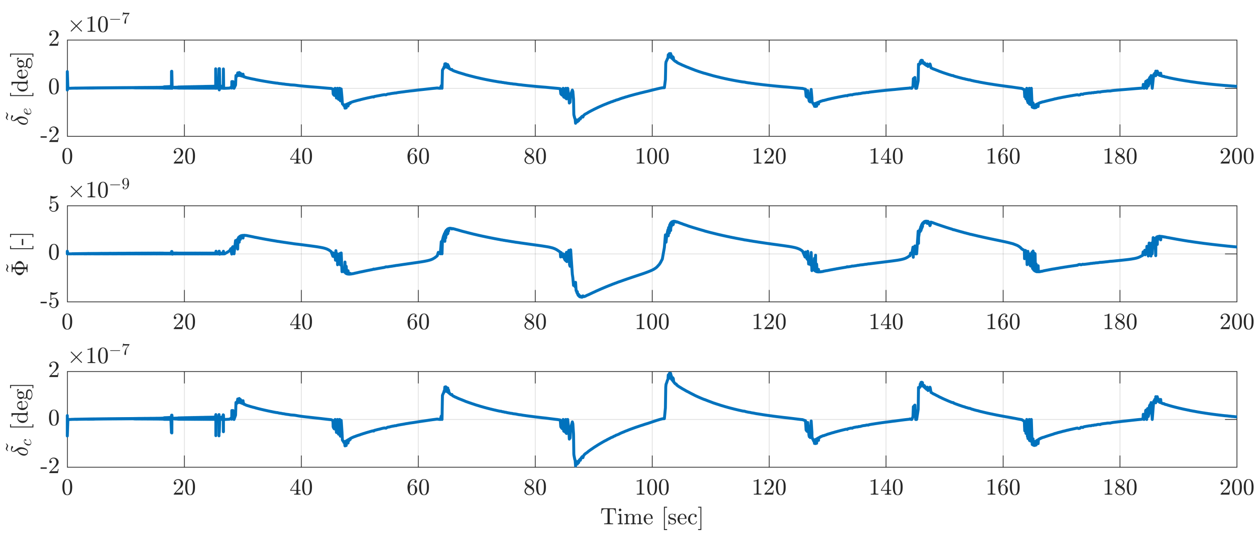

Fig. 5 Control input errors from trim over time. Simulation is initialized exactly at trim conditions. The model used for simulation is the CCOM. Solved with ode23s (stiff Rosenbrock).

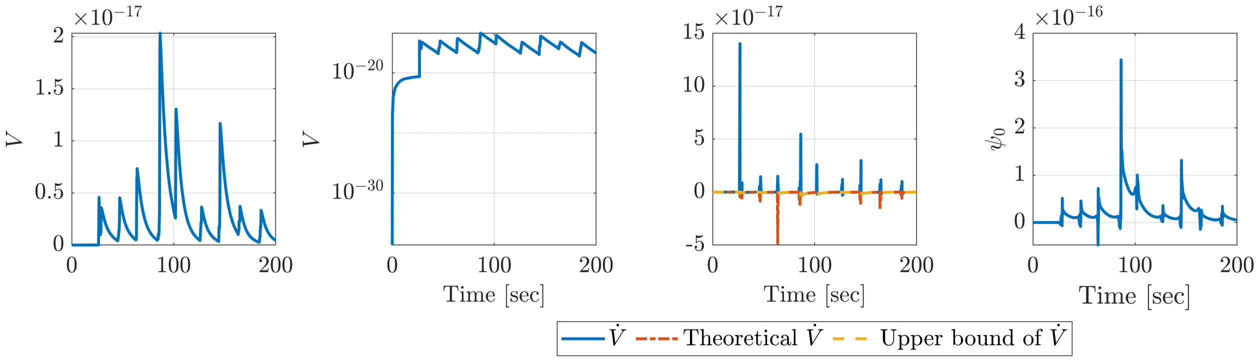

Fig. 6 The Lyaponuv function $V(\tilde{x}) = \tilde{x}^T P\tilde{x}$ (log axis and regular scale), its derivative over time, and ψ_0. Simulation is initialized exactly at trim conditions. The model used for simulation is the CCOM. $\dot{V}$ is the numeric derivative of V along the solution, the theoretical curve is calculated using (7), the upper bound of V is determined according to $-\alpha_V$. $\varepsilon = 0.5$. Solved with ode23s (stiff Rosenbrock).

Next, the controller performance is evaluated when the initial conditions of the system states are deviated from their trim values, i.e., $V_0 = V_t + 200$, [ft/s] and $\alpha_0 = \alpha_t + 2°$. Figures 7 and 8 displays the deviation of $\vec{x}$ from the trim condition ($\tilde{x}$) and corresponding control signal deviations from trim ($\tilde{u}$), respectively. The controller successfully stabilizes the system. One can identify time intervals where some control deviation in $\tilde{u}$ are zero. It agrees with the expected behavior of the RCLF depicted in Fig. 9. It should be noted that although the canard and elevator deflections remain within the operational bounds specified in [2], the value of $\tilde{\Phi}$ becomes unreasonable. $\tilde{\alpha}$, $\tilde{Q}$, and $\tilde{\theta}$ also exceed physically acceptable ranges. Further tuning of the controller could ease the use of control inputs.

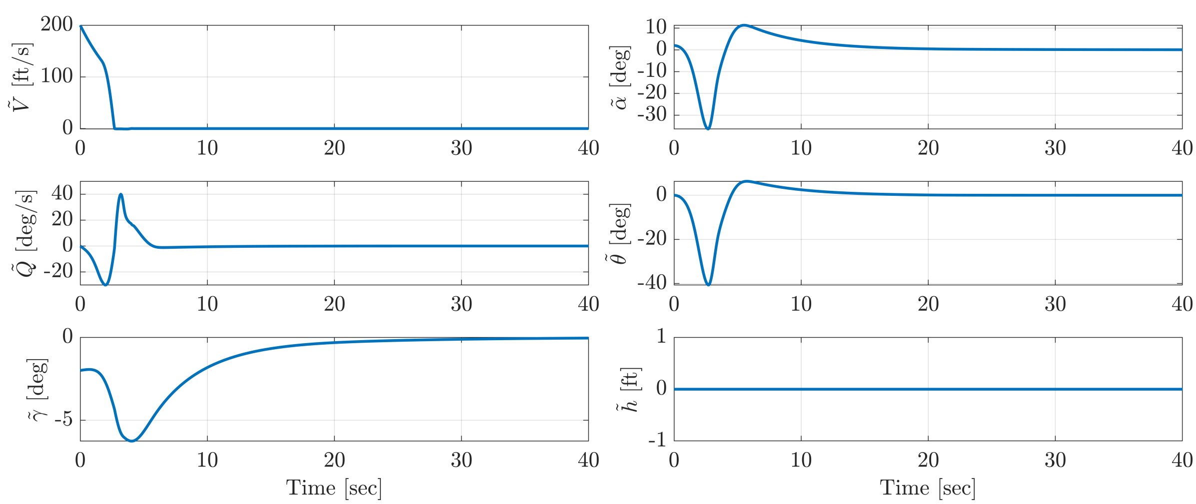

Fig. 7 State errors from trim over time. Simulation is initialized at $V_0 = V_t + 200[ft/s]$, $\alpha_0 = \alpha_t + 2°$. The model used for simulation is the CCOM. Solved with ode4 (Runge Kutta).

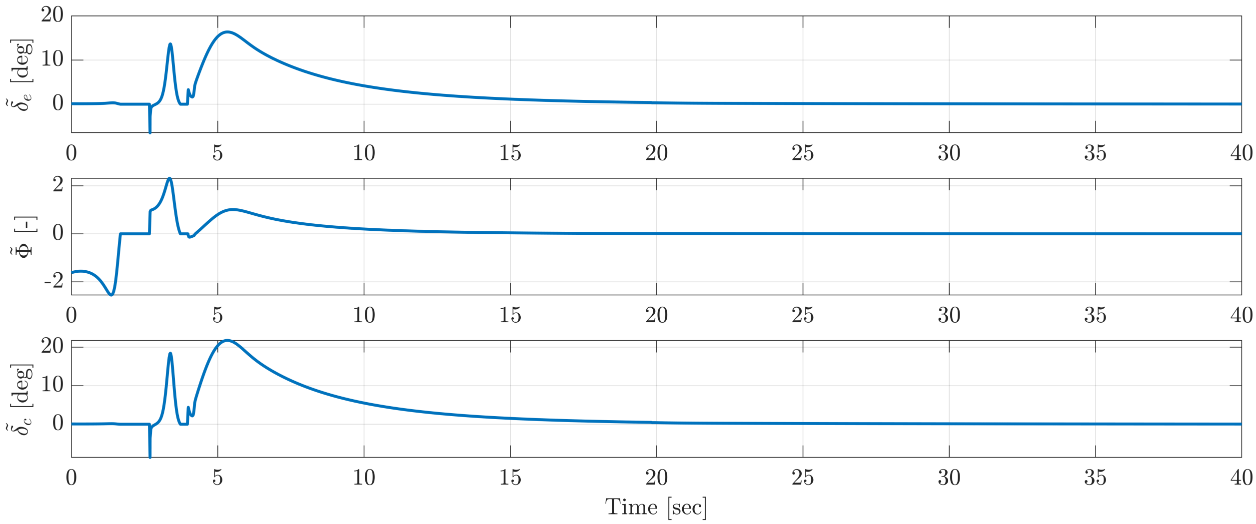

Fig. 8 Control input errors from trim over time. Simulation is initialized at $V_0 = V_t + 200[ft/s]$, $\alpha_0 = \alpha_t + 2°$. The model used for simulation is the CCOM. Solved with ode4 (Runge Kutta).

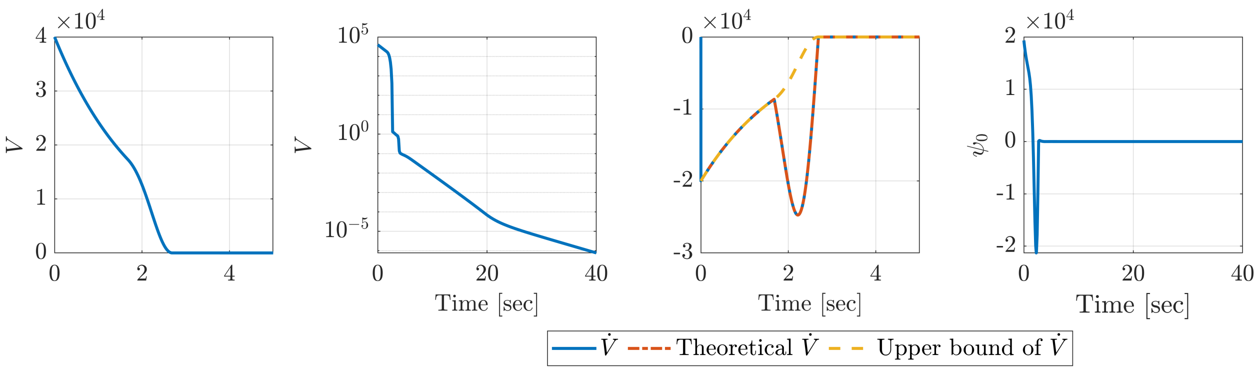

Fig. 9 The Lyaponuv function $V(\tilde{x}) = \tilde{x}^T P \tilde{x}$ (log axis and regular scale), its derivative over time, and ψ_0. Simulation is initialized at $V_0 = V_t + 200[ft/s]$, $\alpha_0 = \alpha_t + 2°$. The model used for simulation is the CCOM. $\dot{V}$ is the numeric derivative of V along the solution, the theoretical curve is calculated using (7), the upper bound of V is determined according to $-\alpha_V$. Solved with ode4 (Runge Kutta).

Figure 9 presents the Lyapunov function $V(\tilde{x}) = \tilde{x}^T P \tilde{x}$ and its derivative over time. A comparison between theoretical derivatives and simulation results is also plotted. As expected, the theoretical and numerical derivatives of $V(\tilde{x})$ agree. In addition, due to the bound in (9), $\dot{V}(\tilde{x})$ doesn't exceed $-\alpha_V$. Between $t \approx 1.8$ [sec] and $t \approx 2.7$ [sec], $\dot{V}(\tilde{x})$ separates from its upper bound, becoming more negative. In this interval, ψ_0 is negative, meaning $V(\tilde{x})$ converges towards the origin even without applying a control signal. Therefore, $\tilde{u}$ is zero within this timeframe. This validates the behavior discussed in Section II. In effect, the choice of ε, Q, and R defines the lower bound of $\dot{V}(\tilde{x})$. Consequently, it is possible to reduce the overall control effort by tuning them.

VI. Conclusions

The PMN control law was discussed and analyzed for an arbitrary feedback linearizable system. To meet its requirements, control-oriented models of the AHV and their controller forms were derived. The PMN law was evaluated via numerical simulations of the system. It performed well for the CCOM, with a reasonable account for the limitations of δ_e and δ_c. However, it violated the physical limitations of the system's states and of Φ. Several controller characteristics were observed, such as chattering around the equilibrium. It was noted that the PMN controller vanishes when it is not required, which displays its core principle. The ECOM, on the other hand, proved to be difficult to control using this method. Although the controller has a strong theoretical basis and all the required conditions of the underlying system model are met, numerical simulations of it failed.

Further work should address the non-linear controls of the model, as well as changes in altitude. A suitable implementation of the PMN control law for the ECOM should be sought. Alternatively, the discrepancy presented earlier must be explained to rule out the use of a PMN law for the ECOM. A solution involving the ECOM could pose a significant development as it would simplify the design and construction of the vehicle. Given the results of numerical simulations, it is also advised to develop a control scheme that prevents the system from leaving the safe range of operation. Seeing as this work is valid only within a 2D world, it should be expanded to a more general 6 degrees-of-freedom problem.

Appendix

A. Coefficient Tables

The following tables refer to the different coefficients that comprise the CFM and COM, according to [2]. Two more tables refer to the flexible modes of the model, but these are of no interest in this paper.

Table A.1 Miscellaneous coefficient values

Coefficient	Value	Units
m	3.0000×10^2	$\mathrm{lb} \cdot \mathrm{ft}^{-1}$
I_y	5.0000×10^5	$\mathrm{lb} \cdot \mathrm{ft}$
S	1.7000×10^1	$\mathrm{ft}^2 \cdot \mathrm{ft}^{-1}$
ρ_0	6.7429×10^{-5}	$\mathrm{slugs} \cdot \mathrm{ft}^{-3}$
h_0	8.5000×10^4	ft
h_s	2.1358×10^4	ft
ω	20.000×10^1	1/s
ζ	7×10^{-1}	—

Table A.2 Drag coefficient values

Coefficient	Value	Units
$C_D^{\alpha^2}$	5.8224×10^0	rad^{-2}
C_D^{α}	-4.5315×10^{-2}	rad^{-1}
$C_D^{\delta_e^2}$	8.1993×10^{-1}	rad^{-2}
$C_D^{\delta_e}$	2.7699×10^{-4}	rad^{-1}
$C_D^{\delta_c^2}$	5.4662×10^{-1}	rad^{-2}
$C_D^{\delta_c}$	1.8466×10^{-4}	rad^{-1}
C_D^{0}	1.0131×10^{-2}	—

Table A.3 Lift coefficient values

Coefficient	Value	Units
C_L^{α}	4.6773×10^{0}	rad^{-1}
$C_L^{\delta_e}$	7.6224×10^{-1}	rad^{-1}
$C_L^{\delta_c}$	5.0816×10^{-1}	rad^{-1}
C_L^{0}	-1.8714×10^{-2}	—

Table A.4 Thrust coefficient values

Coefficient	Value	Units
β_1	-3.7693×10^{5}	$\mathrm{lb} \cdot \mathrm{ft}^{-1} \cdot \mathrm{rad}^{-3}$
β_2	-3.7225×10^{4}	$\mathrm{lb} \cdot \mathrm{ft}^{-1} \cdot \mathrm{rad}^{-3}$
β_3	2.6814×10^{4}	$\mathrm{lb} \cdot \mathrm{ft}^{-1} \cdot \mathrm{rad}^{-2}$
β_4	-1.7277×10^{4}	$\mathrm{lb} \cdot \mathrm{ft}^{-1} \cdot \mathrm{rad}^{-2}$
β_5	3.5542×10^{4}	$\mathrm{lb} \cdot \mathrm{ft}^{-1} \cdot \mathrm{rad}^{-1}$
β_6	-2.4216×10^{3}	$\mathrm{lb} \cdot \mathrm{ft}^{-1} \cdot \mathrm{rad}^{-1}$
β_7	6.3785×10^{3}	$\mathrm{lb} \cdot \mathrm{ft}^{-1}$
β_8	-1.0090×10^{2}	$\mathrm{lb} \cdot \mathrm{ft}^{-1}$

Table A.5 Moment coefficient values

Coefficient	Value	Units
Z_t	8.3600×10^{0}	ft
$\bar{c}$	1.7000×10^{1}	ft
$C_M^{\alpha^2}$	6.2926×10^{0}	rad^{-2}
C_M^{α}	2.1335×10^{0}	rad^{-1}
C_M^{0}	1.8979×10^{-1}	—
c_e	-1.2897×10^{0}	rad^{-1}
c_c	-1.7196×10^{0}	rad^{-1}

References

[1] Freeman, R. A., and Kokotović, P., *Robust Nonlinear Control Design*, Birkhäuser Boston, Boston, MA, 1996. https://doi.org/10.1007/978-0-8176-4759-9, URL http://link.springer.com/10.1007/978-0-8176-4759-9.

[2] Parker, J. T., Serrani, A., Yurkovich, S., Bolender, M. A., and Doman, D. B., "Control-Oriented Modeling of an Air-Breathing Hypersonic Vehicle," *Journal of Guidance, Control, and Dynamics*, Vol. 30, No. 3, 2007, pp. 856–869. https://doi.org/10.2514/1.27830, URL https://arc.aiaa.org/doi/10.2514/1.27830.

[3] Wexler, O., and Idan, M., "Basic Control of a Generic Air-Breathing Hypersonic Vehicle," *Department of Aerospace Engineering, Technion*, 2024. URL https://aerospace.technion.ac.il/wp-content/uploads/2024/11/Omer_Wexler-PROJECT.pdf.